Deep-learning-based reconstruction of undersampled MRI to reduce scan times: a multicentre, retrospective, cohort study

Aditya Rastogi, Gianluca Brugnara, Martha Foltyn-Dumitru, Mustafa Ahmed Mahmutoglu, Chandrakanth J Preetha, Erich Kobler, Irada Pflüger, Marianne Schell, Katerina Deike-Hofmann, Tobias Kessler, Martin J van den Bent, Ahmed Idbaih, Michael Platten, Alba A Brandes, Burt Nabors, Roger Stupp, Denise Bernhardt, Jürgen Debus, Amir Abdollahi, Thierry Gorlia, Jörg-Christian Tonn, Michael Weller, Klaus H Maier-Hein, Alexander Radbruch, Wolfgang Wick, Martin Bendszus, Hagen Meredig, Felix T Kurz, Philipp Vollmuth

Lancet Oncol 2024; 25: 400–10

See Comment page 274

Division for Computational Neuroimaging, Department of Neuroradiology, Heidelberg University Hospital, Heidelberg, Germany (A Rastogi PhD, G Brugnara MD, M Foltyn-Dumitru MD, M A Mahmutoglu MD, C J Preetha MSc, I Pflüger MD, M Schell MD, H Meredig MD, Prof P Vollmuth MD); **Department of Neuroradiology** (A Rastogi, G Brugnara, M Foltyn-Dumitru, M A Mahmutoglu, C J Preetha, I Pflüger, M Schell, Prof M Bendszus MD, H Meredig, Prof P Vollmuth), **Department of Radiation Oncology** (Prof J Debus MD, Prof A Abdollahi MD), **Neurology Clinic** (T Kessler MD, Prof W Wick MD), **Heidelberg Institute of Radiation Oncology** (Prof J Debus, Prof A Abdollahi), **and Heidelberg Ion-Beam Therapy Center** (Prof J Debus, Prof A Abdollahi), **Heidelberg University Hospital, Heidelberg, Germany; Division of Diagnostic and Interventional Neuroradiology, Geneva University Hospitals, Geneva, Switzerland** (Prof F T Kurz MD PhD); **Department of Neuroradiology, University Medical Center Bonn, Rheinische Friedrich-Wilhelms-Universität Bonn, Bonn, Germany** (E Kobler PhD, K Deike-Hofmann MD, Prof A Radbruch MD, Prof P Vollmuth); **Brain Tumor Center at Erasmus MC Cancer Institute, Rotterdam, Netherlands** (Prof M J v d Bent MD); **Assistance Publique-Hôpitaux de Paris, Service de Neurologie 1, Hôpital Pitié-Salpêtrière, Sorbonne Université, Paris, France** (A Idbaih MD); **Department of Neurology, Medical Faculty**

Summary

Background The extended acquisition times required for MRI limit its availability in resource-constrained settings. Consequently, accelerating MRI by undersampling k-space data, which is necessary to reconstruct an image, has been a long-standing but important challenge. We aimed to develop a deep convolutional neural network (dCNN) optimisation method for MRI reconstruction and to reduce scan times and evaluate its effect on image quality and accuracy of oncological imaging biomarkers.

Methods In this multicentre, retrospective, cohort study, MRI data from patients with glioblastoma treated at Heidelberg University Hospital (775 patients and 775 examinations) and from the phase 2 CORE trial (260 patients, 1083 examinations, and 58 institutions) and the phase 3 CENTRIC trial (505 patients, 3147 examinations, and 139 institutions) were used to develop, train, and test dCNN for reconstructing MRI from highly undersampled single-coil k-space data with various acceleration rates (R=2, 4, 6, 8, 10, and 15). Independent testing was performed with MRIs from the phase 2/3 EORTC-26101 trial (528 patients with glioblastoma, 1974 examinations, and 32 institutions). The similarity between undersampled dCNN-reconstructed and original MRIs was quantified with various image quality metrics, including structural similarity index measure (SSIM) and the accuracy of undersampled dCNN-reconstructed MRI on downstream radiological assessment of imaging biomarkers in oncology (automated artificial intelligence-based quantification of tumour burden and treatment response) was performed in the EORTC-26101 test dataset. The public NYU Langone Health fastMRI brain test dataset (558 patients and 558 examinations) was used to validate the generalisability and robustness of the dCNN for reconstructing MRIs from available multi-coil (parallel imaging) k-space data.

Findings In the EORTC-26101 test dataset, the median SSIM of undersampled dCNN-reconstructed MRI ranged from 0·88 to 0·99 across different acceleration rates, with 0·92 (95% CI 0·92–0·93) for 10-times acceleration (R=10). The 10-times undersampled dCNN-reconstructed MRI yielded excellent agreement with original MRI when assessing volumes of contrast-enhancing tumour (median DICE for spatial agreement of 0·89 [95% CI 0·88 to 0·89]; median volume difference of 0·01 cm³ [95% CI 0·00 to 0·03] equalling 0·21%; p=0·0036 for equivalence) or non-enhancing tumour or oedema (median DICE of 0·94 [95% CI 0·94 to 0·95]; median volume difference of –0·79 cm³ [95% CI –0·87 to –0·72] equalling –1·77%; p=0·023 for equivalence) in the EORTC-26101 test dataset. Automated volumetric tumour response assessment in the EORTC-26101 test dataset yielded an identical median time to progression of 4·27 months (95% CI 4·14 to 4·57) when using 10-times-undersampled dCNN-reconstructed or original MRI (log-rank p=0·80) and agreement in the time to progression in 374 (95·2%) of 393 patients with data. The dCNN generalised well to the fastMRI brain dataset, with significant improvements in the median SSIM when using multi-coil compared with single-coil k-space data (p<0·0001).

Interpretation Deep-learning-based reconstruction of undersampled MRI allows for a substantial reduction of scan times, with a 10-times acceleration demonstrating excellent image quality while preserving the accuracy of derived imaging biomarkers for the assessment of oncological treatment response. Our developments are available as open source software and hold considerable promise for increasing the accessibility to MRI, pending further prospective validation.

Funding Deutsche Forschungsgemeinschaft (German Research Foundation) and an Else Kröner Clinician Scientist Endowed Professorship by the Else Kröner Fresenius Foundation.

Introduction

Medical imaging assumes crucial functions across the entire cancer care journey, encompassing tumour diagnosis, staging, treatment planning, monitoring of tumour response, and detection of relapse during follow-up. Nevertheless, access to medical imaging is still

Research in context

Evidence before this study

In the past 5 years, artificial intelligence techniques based on deep convolutional neural networks (dCNN) have demonstrated superior performance compared with conventional reconstruction methods for undersampled MRI and become a subject of great interest. We searched PubMed on July 10, 2023, with no date restrictions on publications, using the search terms ("MRI" OR "magnetic resonance imaging") AND ("oncology") AND ("accelerated" OR "undersampling" OR "undersampled" OR "reconstruction"). No language restrictions were applied to this search. Our search did not identify any articles that evaluated the potential of dCNN-based reconstruction of undersampled MRI in a large multicentre setting or that evaluated its clinical effect on MRI-derived imaging biomarkers in oncology.

Added value of this study

Using our dCNN-based reconstruction of undersampled MRI, we found that substantial reduction of scan times beyond those achieved with conventional MRI acceleration methods is possible, with an acceleration by a factor of 10 demonstrating excellent image quality and accuracy of derived imaging biomarkers for the assessment of oncological treatment response. Moreover, we show excellent generalisability and robustness of the developed dCNN on the public fastMRI benchmark dataset. We provide our developments as open source, which could serve as a blueprint for building similar dCNN-based reconstruction models of undersampled MRI beyond the field of neuro-oncology and thereby guide future clinical translation of accelerating MRI.

Implications of all the available evidence

Our results demonstrate the potential of dCNN-based reconstruction of undersampled MRI data, offering faster MRI scan times without relevantly compromising image quality or accuracy of derived imaging biomarkers for the assessment of oncological treatment response. This advancement holds considerable promise for accelerating MRI, which will be particularly advantageous in resource-constrained settings, and ultimately might increase accessibility to MRI, pending further prospective validation.

limited, with substantial shortages in equipment and workforces, particularly in low-income and middle-income countries. A 2021 *Lancet Oncology* Commission[1] underscored the need to address disparities in medical imaging access and estimated that almost 2·5 million deaths caused by cancer could be prevented through increased access to medical imaging.[1] These disparities are particularly evident for MRI, which is a key imaging method for various cancer types including brain, prostate, and rectal cancer.[2,3] Specifically, accessibility to MRI is low and heterogeneous around the world, with approximately 70% of the world's population having little to no access to MRI, primarily due to its expensive installation, operation, and maintenance costs, as well as the extended acquisition times required for MRI resulting in restricted throughput.[4,5] Various strategies have been developed to shift these boundaries by reducing the acquisition times of MRI, particularly through undersampling of k-space data, which holds the raw MRI data before reconstruction into visually perceivable images.[6] Although conventional MRI acceleration techniques, such as compressed sensing and multi-coil imaging (commonly called parallel imaging), allow acceleration of MRI acquisition by a factor of approximately 2–3,[6–8] higher undersampling is generally avoided to prevent compromising image quality.[9] In the past 5 years, techniques based on deep convolutional neural networks (dCNN) have garnered substantial interest in this field because they have the potential to outperform conventional MRI reconstruction techniques, enabling reconstruction of highly undersampled (ie, highly accelerated) MRI while preserving image quality.[10] Despite encouraging results in methodical proof-of-concept studies, evidence of the potential clinical effect and accuracy of imaging biomarkers derived from highly undersampled MRI in a large-scale setting is currently lacking.[10,11]

Here we report our use of MRI data from three phase 2 or phase 3 clinical trials, with more than 2000 patients with glioblastoma from over 200 unique institutions overall, to develop, train, and test the potential of a dCNN optimisation method for reconstruction of highly undersampled MRI. Additionally, we used the public NYU Langone Health fastMRI brain dataset with 558 patients from five institutions, covering a broad disease spectrum on neuroimaging, to further validate the generalisability and robustness of the developed dCNN. With this dCNN we aimed to substantially reduce scan times beyond those achieved with conventional MRI acceleration methods, and to assess its impact on image quality and the accuracy of MRI-derived imaging biomarkers.

Methods

Study design and data sources

In this multicentre, retrospective, cohort study, we analysed MRI data from patients with glioblastoma acquired at the Heidelberg University Hospital (HD cohort) and from the multicentre phase 2 CORE trial (CORE cohort),[12] the multicentre phase 3 CENTRIC trial (CENTRIC cohort),[13] and the phase 2/3 European Organisation for Research and Treatment of Cancer (EORTC) 26101 trial (EORTC-26101 cohort).[14,15] We selected all MRI scans that were acquired within the

Mannheim, Mannheim Center for Translational Neuroscience, University of Heidelberg, Mannheim, Germany (Prof M Platten MD); **Clinical Cooperation Unit Neuroimmunology and Brain Tumor Immunology** (Prof M Platten) **and Clinical Cooperation Unit Neurooncology** (T Kessler, Prof W Wick), **German Cancer Consortium within German Cancer Research Center, Heidelberg, Germany; Department of Medical Oncology, Azienda Unità Sanitaria Locale of Bologna, Bologna, Italy** (Prof A A Brandes MD); **Department of Neurology, Division of Neuro-Oncology, University of Alabama at Birmingham, Birmingham, AL, USA** (Prof B Nabors MD); **O'Neal Comprehensive Cancer Center, University of Alabama at Birmingham, Birmingham, AL, USA** (Prof B Nabors); **Lou and Jean Malnati Brain Tumor Institute, Robert H Lurie Comprehensive Cancer Center** (Prof R Stupp MD), **Department of Neurological Surgery** (Prof R Stupp), **and Department of Neurology** (Prof R Stupp), **Northwestern Medicine and Northwestern University, Chicago, USA; Department of Radiation Oncology, School of Medicine and Klinikum rechts der Isar, Technical University of Munich, Munich, Germany** (D Bernhardt MD); **European Organization for Research and Treatment of Cancer, Brussels, Belgium** (T Gorlia PhD); **Department of Neurosurgery, Ludwig-Maximilians-University, Munich, Germany** (Prof J-C Tonn MD); **German Cancer Consortium within German Center Research Center, partner site Munich, Germany** (Prof J-C Tonn); **Department of Neurology, University Hospital and University of Zurich, Zurich, Switzerland** (Prof M Weller MD); **Medical Image Computing** (Prof K H Maier-Hein PhD Prof P Vollmuth) **and Department of Radiology** (Prof F T Kurz) **German Cancer Research Center, Heidelberg, Germany; Pattern Analysis and Learning Group, Department of Radiation Oncology, Heidelberg University Hospital, Heidelberg, Germany** (Prof K H Maier-Hein); **German**

Center for Neurodegenerative Diseases, Bonn, Germany
(K Deike-Hofmann)

Correspondence to:
Prof Philipp Vollmuth, Division for Computational Neuroimaging, Department of Neuroradiology, Heidelberg University Hospital, 69120 Heidelberg, Germany
p.vollmuth@dkfz-heidelberg.de

CORE, CENTRIC, and EORTC-26101 studies. Available MRI scans were excluded (ie, classified as not assessable) if any of the following criteria were met: corrupt data following DICOM to NIfTI file conversion (primarily due to the non-standardised centre-specific anonymisation of DICOM files) or reading; errors upon loading the NIfTI files; incomplete availability of T1-w, cT1-w, FLAIR, and T2-w sequences (requiring either 3D acquisitions or 2D with axial orientation); or heavy motion artifacts, precluding adequate image co-registration. Additionally, we retrospectively analysed brain MRI from the fastMRI initiative database (fastMRI brain cohort).[16] No exclusion criteria were applied to the fastMRI dataset. The study cohorts and the analysis workflow are shown in figure 1. A detailed description of all study cohorts and inclusion and exclusion criteria are in the appendix (pp 4–5, 11–12).

See Online for appendix

Retrospective evaluation was approved by the local ethics committee of the University of Heidelberg and informed consent was waived; evaluation of the CENTRIC, CORE, and EORTC-26101 cohorts was granted through an external research project with the EORTC. Evaluation of the fastMRI brain cohort was performed in accordance with the fastMRI Dataset Sharing Agreement. Specifically, the fastMRI investigators provided data but did not participate in analysis or writing of this study. The primary goal of fastMRI is to test whether machine learning can aid in the reconstruction of medical images.

For more on the **fastMRI investigators** see https://fastmri.med.nyu.edu

Procedures

The analysis workflow complies with the CLAIM and STROBE guidelines.[17,18] In this study, we used a physics-based neural network—namely, Model Based Deep Learning Architecture for Inverse Problems.[19] These architectures explicitly include the physical relationship between the observed data (ie, the undersampled k-space data) and the object that was measured (ie, the desired data, in this case the high-quality MRI sequences). This architecture combines classic iterative techniques of solving inverse problems with deep learning. The network consists of two modules, one enforces the physical relationship between undersampled k-space data and the required anatomical image and a second deep learning-based module that learns features of the anatomical image to aid in reconstruction. A detailed description of the mathematical framework and the architecture of the dCNN is in the appendix (pp 2–4, 24).

The same image processing steps were applied to all MRI sequences. First, individual MRI sequences within the HD, CENTRIC, CORE, and EORTC-26101 cohorts were retrospectively converted into simulated raw k-space data by using 2D or 3D fast Fourier transform. No information from coil sensitivity maps or coil images were available due to retrospective data acquisition, which required treating the retrospectively generated k-space data as a single-coil acquisition. For the fastMRI brain cohort, multi-coil raw k-space data were prospectively available and additional single-coil k-space data were retrospectively simulated, as described in the appendix (p 5). Subsequently, the k-space data were undersampled by a factor of R=2, 4, 6, 8, 10, and 15 (designated as R=2–15) using the radial golden angle undersampling mask.

Next, the dCNN models were trained with all MRI data from the HD, CENTRIC, and CORE cohorts to reconstruct original MRI from the undersampled k-space data with separate models trained for each undersampling rate (R=2–15) and for each sequence modality (T1-w, cT1-w, FLAIR, and T2-w), as described in the appendix (p 5). The trained dCNN models were tested (without retraining) for reconstructing original MRIs from the undersampled k-space data in the EORTC-26101 and fastMRI brain cohorts. Within both cohorts, the quality of the undersampled dCNN-reconstructed MRI (for each undersampling rate of R=2–15) with the corresponding original MRI (R=0) was quantified with standard image quality metrics,[16,20] including structural similarity index measure (SSIM; calculated on magnitude values [non-negative]), high frequency error norm (HFEN), peak signal-to-noise ratio (PSNR), and root mean squared error (RMSE). For SSIM (for which the maximum value is 1 if the two images are identical) and PSNR, a higher value denotes better quality, whereas for RMSE and HFEN, a lower value denotes better quality of the undersampled dCNN-reconstructed MRI.

The accuracy of undersampled dCNN-reconstructed MRI on downstream radiological assessment of imaging biomarkers in oncology was evaluated within the EORTC-26101 cohort. First, automated tumour segmentation was performed as described previously[21] using a trained 3D U-Net convolutional neural network model using T1-w, cT1-w, FLAIR, and T2-w sequences as input. This process was separately performed seven times using original MRI (R=0) or dCNN-reconstructed MRI from each undersampling rate (R=2–15) as input. Thereby volumetric segmentation masks with delineation of the contrast-enhancing tumour and the non-enhancing T2/FLAIR hyperintense abnormality, excluding the contrast-enhancing and necrotic portion of the tumour, resection cavity, and leukoaraiosis, were generated. Subsequently, volumetric tumour response assessment was performed,[21] including calculation of the time to progression by analysing the longitudinal change in the contrast-enhancing tumour volumes and the T2/FLAIR signal abnormality (referred to as non-enhancing tumour or oedema) volumes for each patient.

Outcomes

The present study had three main objectives. First, to evaluate the quality of the undersampled dCNN-reconstructed MRI compared with the original MRI within the EORTC-26101 and fastMRI brain cohort using standard quantitative metrics. Second, to assess the

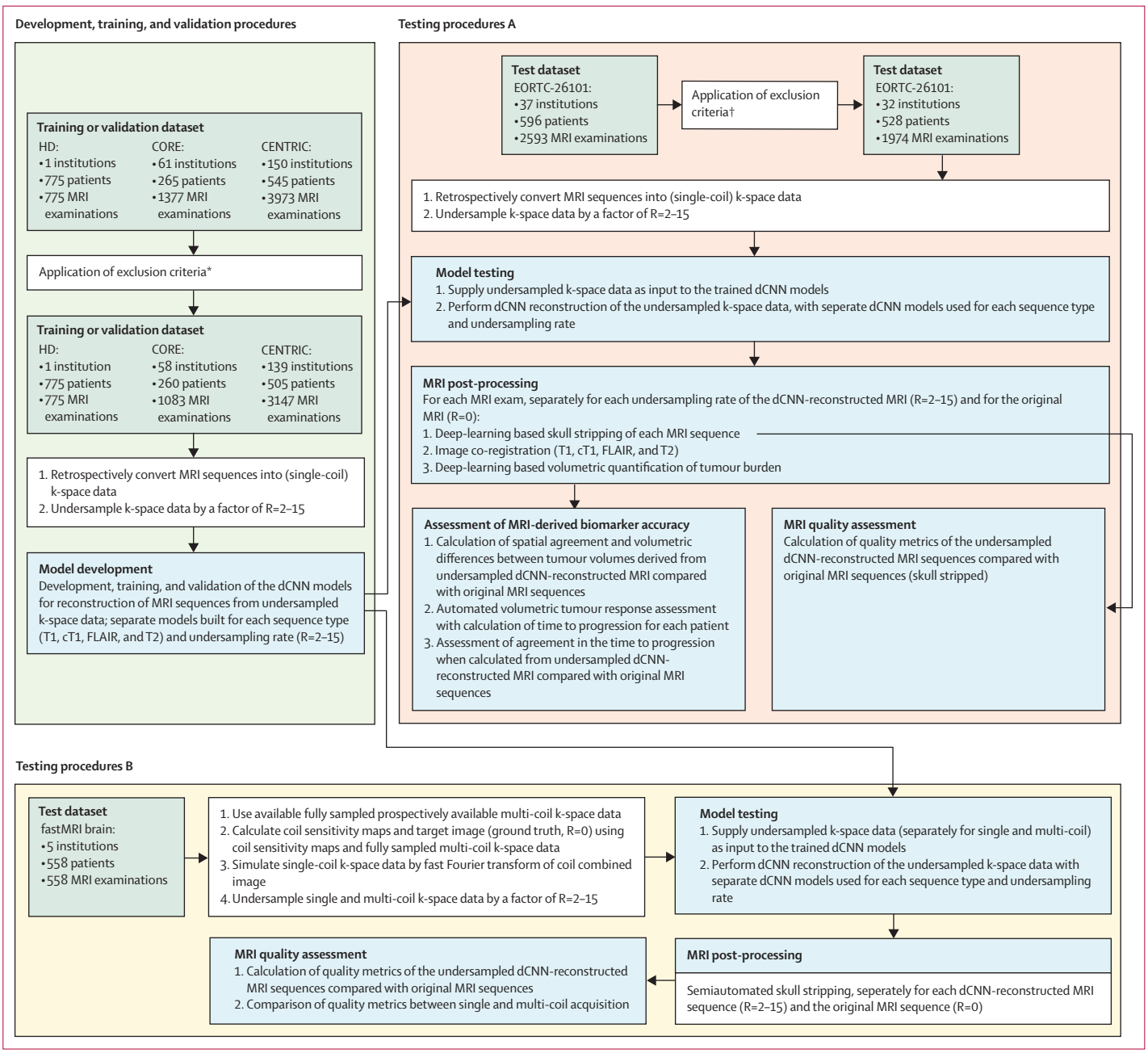

Figure 1: **Procedures for the development, training, validation, and independent testing of the dCNN optimisation method for MRI reconstruction and assessment of its clinical impact on MRI-derived imaging biomarkers in oncology**

cT1=contrast-enhanced T1-weighted. dCNN=deep convolutional neural network. EORTC=European Organisation for Research and Treatment of Cancer. FLAIR=fluid attenuated inversion recovery. HD=Heidelberg University Hospital cohort. T1T1-weighted. T2=T2-weighted. TTP=time to progression. *302 examinations with corrupt MRI data, 741 examinations with missing MRI sequences, and 77 examinations with heavy motion artifacts. †238 examinations with corrupt MRI data, 374 examinations with missing MRI sequences, and seven examinations with heavy motion artifacts.

accuracy of undersampled dCNN-reconstructed MRI on downstream radiological assessment of imaging biomarkers in the EORTC-26101 cohort compared with the original MRI by quantifying the spatial and volumetric agreement, separately for contrast-enhancing tumour and non-enhancing tumour or oedema volumes, and by quantifying the accuracy of derived tumour response assessment measurements (time to progression), which is a central imaging biomarker in oncology. Third, to assess the generalisability and robustness of the developed dCNN within the fastMRI brain cohort, by applying it to prospectively available k-space data with comparison of the performance of the dCNN for both single-coil and multi-coil MRI acquisition scenarios.

Statistical analysis

The cohort size for each of the included datasets was determined by availability of samples and not derived from a power calculation. The quality of the dCNN-reconstructed MRI in the EORTC-26101 and fastMRI brain cohorts was separately quantified for each undersampling rate (R=2–15) using SSIM, HFEN, PSNR, and RMSE metrics. In the EORTC-26101 cohort the agreement between tumour volumes derived from original MRIs compared with dCNN-reconstructed MRIs was evaluated (separately for each undersampling rate of R=2–15) with the DICE similarity coefficient for spatial agreement and Bland-Altman plots for volume agreement. A Wilcoxon signed-rank test for equivalence using a two one-sided tests (known as TOST) procedure was applied to evaluate equivalence in tumour volume measurements within the EORTC-26101 cohort when derived from original MRI compared with the dCNN-reconstructed MRI. This analysis was conducted separately for each undersampling rate (R=2–15) after confirming the primary assumption of the test—namely, the symmetrical distribution of differences between paired measurements. An equivalence bound of 0·1 cm^3 was set for contrast-enhancing tumour volumes and 1 cm^3 for non-enhancing tumour or oedema volumes.

Kaplan–Meier plots and log-rank tests were generated for the EORTC-26101 cohort to assess the association in time to progression on a group level when using original MRI versus dCNN-reconstructed MRI. Time to progression was calculated from the date of baseline MRI in the EORTC-26101 trial until the date of tumour progression on MRI; patients were only included if they had a baseline and at least one follow-up MRI and censoring was done at the date of the last MRI if no progression occurred during follow-up. Progression was defined, as described previously,[21] as an increase in the contrast-enhancing tumour volume by 40% (which corresponds to an increase of the area of contrast enhancing tumour by 25% determined by bi-perpendicular tumour diameters as defined by response assessment in neuro-oncology [RANO] criteria[22]) or as an increase in the non-enhancing tumour or oedema volumes by 100% compared with baseline or best response. Moreover, agreement in time to progression (considering both time-to-event and censoring status) was assessed on an individual level with calculation of Cohen's kappa coefficient (with two levels), which takes into account the possibility of the agreement occurring by chance.

Within the fastMRI brain cohort, a Wilcoxon signed-rank test (with calculation of effect sizes) was used to evaluate (separately for each undersampling rate of R=2–15) whether the quality metrics derived from multi-coil MRI acquisition are different from those derived from single-coil MRI acquisition. Moreover, to objectively compare the performance between the EORTC-26101 cohort (single-coil acquisition) and the fastMRI brain cohort (single-coil acquisition), the SSIM was used as a target metric because it is a bounded metric (–1 to 1) and less influenced by the different intensity scales of the generated MRI sequences stemming from prospective (fastMRI) versus retrospectively (EORTC-26101) generated k-space data than the other metrics (appendix p 6). Specifically, a Wilcoxon-Mann-Whitney test (with calculation of effect sizes) was used to evaluate (separately for each undersampling rate of R=2–15) whether the SSIM derived from single-coil acquisitions is different between the EORTC-26101 and the fastMRI brain cohort. Moreover, the performance of the dCNN for reconstruction of MRI from multi-coil acquisition in the fastMRI brain cohort was compared with the official leader-board of the best performing algorithms in the FastMRI 2020 challenge (with SSIM as the target metric; appendix p 7).[10] Linear mixed-effects models were generated to assess the influence of different undersampling rates (R value) on the evaluated metrics. For this purpose, the R value was treated as a fixed effect, whereas the MRI examinations were treated as a random effect (to account for the repeated measurements obtained for separate R values within each examination). Linear regression models were generated to assess the influence of tumour volumes on the DICE coefficient for spatial agreement (separately for each R value). The reported 95% CIs for the median of the assessed metrics were calculated using non-parametric bootstrap resampling (percentile method) with n=1000 iterations.

A p value of less than 0·05 was considered significant. Statistical analyses were done with R version 4.3.1, Matlab version R2022b (MathWorks, Natick, MA, USA), and Python version 3.10 (Python Software Foundation, Beaverton, OR, USA).

Role of the funding source

The funder had no role in study design, data collection, data analysis, data interpretation, or writing of the report.

Results

The compiled MRI from patients with glioblastoma being treated at Heidelberg University Hospital (775 patients with one examination each, recruited between July, 2009, and August, 2019) and within the multi-institutional longitudinal phase 2 CORE trial (260 patients with 1083 examinations from 58 institutions, recruited between March, 2009, and February, 2013) and phase 3 CENTRIC trial (505 patients with 3147 examinations from 139 institutions, recruited between September, 2008, and November, 2012) were allocated for training and validation of dCNN models reconstructing MRI from highly undersampled k-space data (figure 1; demographic, clinical, and MRI characteristics of cohorts are in the appendix pp 11–12). Independent testing of the dCNN models on the multi-institutional longitudinal phase 2/3 EORTC-26101 trial (528 patients with 1974 examinations from 32 institutions; recruited between October, 2011,

and December, 2015; appendix pp 11–12) yielded a median SSIM score (ie, similarity between original MRI and undersampled dCNN reconstructed MRI) ranging from 0·88 to 0·99 across the evaluated undersampling rates of R=2–15, with 0·92 (95% CI 0·92–0·93) for 10-times undersampling (R=10). Detailed results for each undersampling rate (and for additional quality metrics, such as PSNR, HFEN, and RMSE) are in the appendix (pp 16, 25). Linear mixed-effects models demonstrated that the quality of the dCNN-reconstructed MRI sequences decreased for higher undersampling rates (p<0·0001 each; appendix p 23). Specifically, the changes in the undersampling rate were responsible for explaining 22–44% of the variation (marginal R^2) in the quality metrics of the dCNN-reconstructed MRI. The dCNN required a median of 1·3 s (95% CI 1·2–1·4) to reconstruct a 2D MRI and 3·3 s (3·1–3·4) to reconstruct a 3D MRI from undersampled k-space data (appendix p 7). An illustrative case from the EORTC-26101 test set depicting the original MRI and the undersampled MRI without or with dCNN reconstruction across all evaluated undersampling rates (R=2–15) is shown in the appendix (pp 26).

Automated segmentation of tumour burden in the EORTC-26101 test set yielded a median contrast-enhancing tumour volume of 5·74 cm³ (95% CI 5·14 to 6·51) and a median non-enhancing tumour or oedema volume of 44·60 cm³ (42·30 to 46·54) when derived from original MRI sequences with R=0. When using the corresponding undersampled dCNN reconstructed MRI for assessing the tumour burden in the EORTC-26101 test set, the contrast-enhancing tumour volume showed a median difference (compared with R0) ranging from –0·15 cm³ to 0·01 cm³ (corresponding to a median underestimation or overestimation of –2·66% to 0·21%) across the evaluated undersampling rates of R=2–15 (figure 2; appendix p 17). Similarly, for the non-enhancing tumour or oedema volumes the median difference (compared with R0) ranged from –0·79 cm³ to –0·01 cm³ (corresponding to a median underestimation of –1·77% to –0·01%) across the evaluated undersampling rates of R=2–15 (figure 2; appendix p 17). The corresponding Bland-Altman plots are in the appendix (pp 27–28). The median DICE coefficients (for spatial agreement between tumour volumes derived from original MRI *vs* undersampled dCNN-reconstructed MRI) ranged from 0·85 to 0·97 for contrast-enhancing tumour and from 0·91 to 0·98 for non-enhancing tumour or oedema (appendix p 29). Spatial agreement for both contrast-enhancing tumour and non-enhancing tumour or oedema volumes was higher for larger tumour volumes across all undersampling rates (p<0·0001 each; appendix pp 30–31). Details on false positives and false negatives regarding the detection of contrast-enhancing tumour and non-enhancing tumour or oedema volumes from undersampled dCNN reconstructed MRI is shown in the appendix (p 21).

Equivalence in contrast-enhancing tumour volume measurements derived from undersampled dCNN-reconstructed MRI compared with original MRI within the EORTC-26101 test set was established for undersampling rates of R=2–10 (p≤0·036), but not for R=15 (p>0·99; appendix p 17). For non-enhancing tumour or oedema volume, equivalence of measurements derived from undersampled dCNN-reconstructed MRI compared with original MRI was established for all evaluated undersampling rates of R=2–15 (p≤0·023; appendix p 17). Consequently, R=10, which was the highest undersampling rate whereby equivalence for both contrast-enhancing tumour and non-enhancing tumour or oedema volumes was established, was chosen as the value with the best trade-off for further downstream

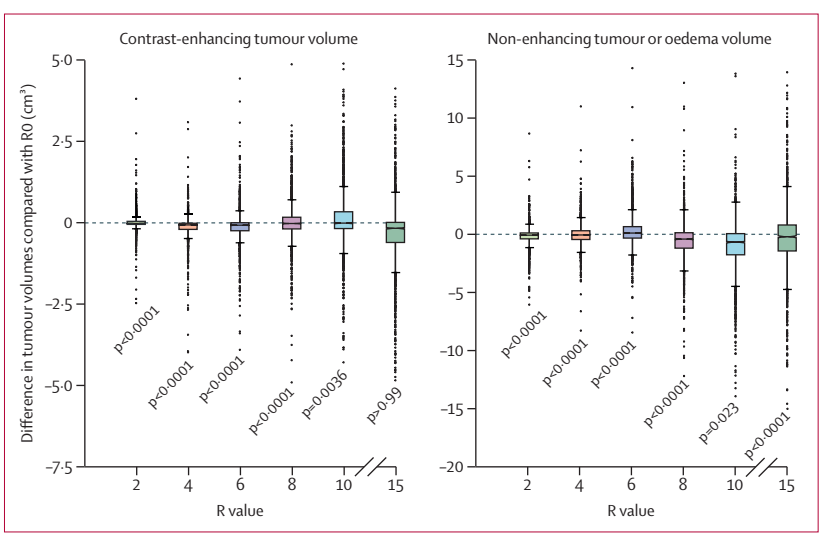

Figure 2: **Absolute difference in tumour volumes derived from undersampled dCNN-reconstructed MRI sequences across different acceleration rates (R value) compared with those derived from the original MRI sequences**

dCNN=deep convolutional neural network. p values were derived from a Wilcoxon signed-rank test for equivalence using a two one-sided tests (known as TOST) procedure. The dashed horizontal line corresponds to a zero difference in tumour volumes. For each boxplot, the upper and lower bounds of the boxes show IQR and the horizontal central line shows the median. The sides of boxplots are indented to indicate the 95% CI of the median. Whiskers represent 1·5 times the IQR. Dots are outliers.

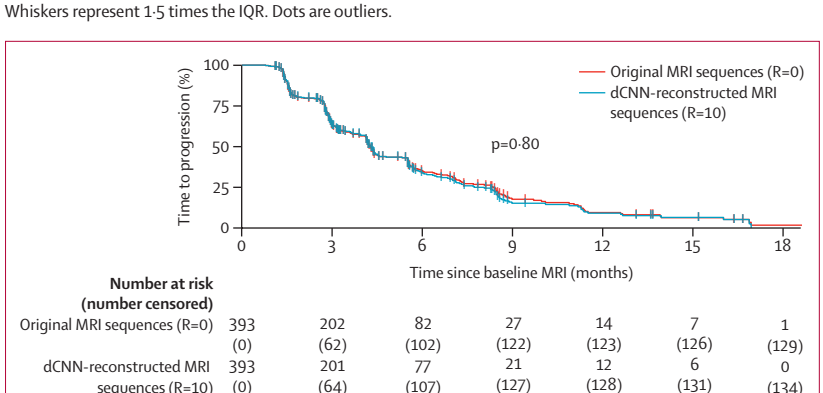

Number at risk (number censored)							
Original MRI sequences (R=0)	393 (0)	202 (62)	82 (102)	27 (122)	14 (123)	7 (126)	1 (129)
dCNN-reconstructed MRI sequences (R=10)	393 (0)	201 (64)	77 (107)	21 (127)	12 (128)	6 (131)	0 (134)

Figure 3: **Kaplan–Meier estimates for time to progression in the EORTC-26101 test set when performing automated volumetric tumour response assessment on undersampled dCNN-reconstructed MRI sequences (with 10-times acceleration; R=10) versus original MRI sequences (R=0)**

dCNN=deep convolutional neural network. EORTC=European Organisation for Research and Treatment of Cancer.

analysis. Specifically, the 10-times undersampled dCNN-reconstructed MRI yielded excellent agreement with original MRI when assessing volumes of contrast-enhancing tumour (median DICE for spatial agreement of 0·89 [95% CI 0·88 to 0·89]; median volume difference of 0·01 cm³ [95% CI 0·00 to 0·03] equalling 0·21%; p=0·0036 for equivalence) and non-enhancing tumour or oedema (median DICE of 0·94 [95% CI 0·94 to 0·95]; median volume difference of –0·79 cm³ [95% CI –0·87 to –0·72] equalling –1·77%; p=0·023 for equivalence; figure 2; appendix p 17). When assessing contrast-enhancing tumour volumes on 10-times undersampled dCNN-reconstructed MRI, the rate of false negatives was 18 (0·91%) of 1974 (with a median volume on original MRI of 0·110 cm³ [range 0·003 to 0·331]) and the rate of false positives was 26 (1·32%) of 1974 (with a median volume on 10-times undersampled dCNN-reconstructed MRI of 0·068 cm³ [range 0·005 to 2·344]). The rate of false negatives and false positives when assessing non-enhancing tumour or oedema volumes on 10-times undersampled dCNN-reconstructed MRI was both 0 (0%) of 1974 (appendix p 21).

Volumetric tumour response assessment in a subset of the EORTC-26101 test set with available baseline and subsequent follow-up MRI (393 [74%] of 528 patients, with a median follow-up time of 8·9 months [IQR 6·1 to 12·7]) showed a median time to progression of 4·27 months (95% CI 4·14 to 4·57) when derived from original MRI and 4·27 months (4·14 to 4·57) when derived from 10-times undersampled dCNN-reconstructed MRI (log-rank p=0·80; figure 3; table). Specifically, with R=10 the agreement in the time to progression (considering both time to event and censoring status) was found in 374 of 393 patients (95·2% [95% CI 92·6 to 96·9] with a Cohen´s kappa coefficient of 0·89 [95% CI 0·85 to 0·94] indicating almost perfect agreement;[23] table). For patients with disagreement (19 [4·8%] of 393 patients), tumour progression was detected at a later timepoint with 10-times undersampled dCNN-reconstructed MRI than with the original MRI in four (1%) of 393 patients (median difference in the time to progression of 2·35 months [95% CI 1·35 to 4·37]) and at an earlier timepoint in nine (2·3%) of 393 patients (median difference in the time to progression of –4·57 months [95% CI –2·76 to –5·56]). Additionally, tumour progression not evident on original MRI was found in one (0·3%) of 393 patients with 10-times undersampled dCNN-reconstructed MRI. Furthermore, tumour progression evident on original MRI was not found in five (1·3%) of 393 patients with 10-times undersampled dCNN-reconstructed MRI. Results for the remaining undersampling rates are in the table and the appendix (p 32).

The whole fastMRI brain cohort test dataset (558 patients with 558 examinations; figure 1) was used without any exclusion criteria to validate how well the developed dCNN generalises (without retraining) to the prospectively available k-space data from the fastMRI brain cohort. This cohort included a variety of patients, with the most prevalent category on MRI being normal for age (ie, no pathology) in 253 (45%) of 558 patients, followed by presence of non-specific white matter lesions in 69 (12%), and mass lesions in 34 (6%; appendix p 22;

	R=2	R=4	R=6	R=8	R=10	R=15
Case-level agreement						
Agreement, n	381	377	374	375	374	364
% (95% CI)	97·0% (94·7–98·2)	96·9% (94·7–98·2)	95·2% (92·6–96·9)	95·4% (92·9–97·1)	95·2% (92·6–96·9)	92·6% (89·6–94·8)
Kappa (95% CI)	0·93 (0·89–0·97)	0·93 (0·89–0·97)	0·89 (0·85–0·94)	0·90 (0·85–0·94)	0·89 (0·85–0·94)	0·84 (0·78–0·90)
Disagreement, n (%)	2 (3·1%)	12 (3·1%)	19 (4·8%)	18 (4·6%)	19 (4·8%)	29 (7·5%)
No progression with dCNN-reconstituted MRI, but with original MRI	3 (0·8%)	3 (0·8%)	5 (1·3%)	2 (0·5%)	5 (1·3%)	5 (1·3%)
Progression with dCNN-reconstituted MRI, but not with original MRI	0	0	2 (0·5%)	1 (0·3%)	1 (0·3%)	3 (0·8%)
Later progression with dCNN-reconstituted MRI compared with original MRI	6 (1·5%)	3 (0·8%)	7 (1·8%)	7 (1·8%)	4 (1·0%)	6 (1·5%)
Earlier progression with dCNN-reconstituted MRI compared with original MRI	3 (0·8%)	6 (1·5%)	5 (1·3%)	8 (2·0%)	9 (2·3%)	15 (3·8%)
Cohort-level agreement						
TTP from original MRI (R=0), median (95% CI)	4·27 (4·14–4·57)	4·27 (4·14–4·57)	4·27 (4·14–4·57)	4·27 (4·14–4·57)	4·27 (4·14–4·57)	4·27 (4·14–4·57)
TTP from dCNN-reconstituted MRI, median (95% CI)	4·31 (4·14–5·52)	4·27 (4·14–4·57)	4·31 (4·14–5·52)	4·27 (4·14–4·80)	4·27 (4·14–4·57)	4·21 (4·14–4·50)
Log-rank, p value	0·84	0·96	0·84	0·92	0·80	0·80

Agreement for the time to progression (considering both time to progression and censoring status) is shown on an individual case basis (case-level agreement) and for the overall cohort (cohort-level agreement) using Kaplan–Meier estimates and log-rank testing (between time to progression curves obtained from undersampled dCNN-reconstructed MRI *vs* original MRI). dCNN=deep convolutional neural network. EORTC=European Organisation for Research and Treatment of Cancer.

Table: **Agreement in time to progression within the EORTC-26101 cohort (N=393) when obtained from undersampled dCNN-reconstructed MRI across different acceleration rates (R value) compared with that obtained from original MRI (R=0)**

MRI characteristics are shown in the appendix [pp 11–12]). The demographic details of the fastMRI brain cohort test dataset are not publically available. To objectively compare the image quality between the EORTC-26101 and fastMRI brain cohort for single-coil acquisition, the SSIM was used as a target metric to shown generalisability of the dCNN. Specifically, the SSIM was significantly higher in the fastMRI brain cohort with single-coil acquisition ($p<0·0001$ each) than in the EORTC-26101 single-coil acquisition test set, although effect sizes were small (ranging from 0·08 [95% CI 0·07 to 0·09] to 0·17 [0·16 to 0·19]) across different undersampling rates (figure 4; appendix p 19). Moreover, within the fastMRI brain cohort, the generalisability of the developed dCNN to a multi-coil acquisition scenario was assessed. For this purpose, comparison of the quality from dCNN reconstructed MRI stemming from single-coil versus multi-coil k-space data showed significant improvements in the SSIM across different undersampling rates, when using multi-coil acquisition ($p<0·0001$ each; figure 4; appendix p 19). The largest effect size, 0·87 (95% CI 0·87 to 0·87), was observed at the lowest undersampling rate (R=2), and the smallest effect size, 0·25 (0·18 to 0·33), was noted at the highest undersampling rate (R=15). Results for each undersampling rate (and for additional metrics including PSNR, HFEN, and RMSE) comparing single-coil versus multi-coil k-space data in the fastMRI brain cohort are in the appendix (pp 18, 33). The SSIM results from the leaderboard of the 2020 fastMRI challenge[10] were used as a reference or benchmark to compare the quality of multi-coil reconstruction using dCNN (appendix p 20). Even though the developed dCNN was not trained on the multi-coil fastMRI dataset, the performance was on par with the top-performing algorithms of the FastMRI challenge and thereby support its generalisability to settings with prospectively available k-space data (appendix pp 7, 20). An illustrative case from the fastMRI cohort depicting the real, imaginary, and magnitude of the complex original MRI as well as the undersampled MRI without and with dCNN reconstruction across all evaluated undersampling rates (R=2–15) is in the appendix (pp 34–37).

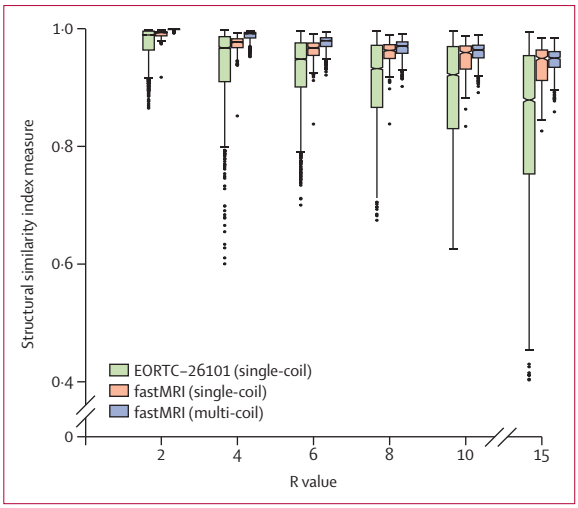

Figure 4: **Structural similarity index measure of dCNN-reconstructed MRI across different acceleration rates (R value) compared with original MRI in the EORTC-26101 (single-coil acquisition) and fastMRI brain (separately for single-coil and multi-coil acquisition) test datasets.**
dCNN=deep convolutional neural network. EORTC=European Organisation for Research and Treatment of Cancer. For each boxplot, the upper and lower bounds of the boxes show the IQR of datapoints, with the horizontal central line showing the median. The sides of blocks are indented to indicate the 95% CI of the median. Whiskers represent 1·5 times the IQR. Dots are outliers.

Discussion

By incorporating MRI data from three phase 2 or 3 clinical trials in neuro-oncology alongside retrospective institutional data, with more than 2000 patients with glioblastoma from over 200 unique institutions overall, for training and independent testing of the dCNN, we show excellent test-time performance both in image quality metrics and accuracy of derived imaging biomarkers for the assessment of oncological treatment response when derived from 10-times undersampled dCNN-reconstructed MRI, when compared with original MRI. Moreover, we show the generalisability and robustness of the developed dCNN on the public fastMRI dataset, with 558 patients from five institutions, covering a broad disease spectrum on neuroimaging, achieving excellent performance in terms of image quality on prospectively available k-space data. From a practical perspective, the 10-times undersampling would translate into an acceleration in MRI scan time by a factor of 10 when using single-coil acquisition and a factor of 3·3 to 5·0 when using multi-coil (parallel) acquisition. These advances might not only contribute to increasing patient throughput and, consequently, accessibility to MRI, but also benefit diagnostic accuracy by reducing the probability of patient motion artifacts—a well known problem in MRI—through shorter acquisition times.

Our results exemplify that dCNN-based reconstruction techniques can enable us to push the limits of reconstruction performance and acceleration of MRI.[24,25] Conceptually, these dCNN-based approaches can be roughly divided into two categories: purely data-driven and model-driven. Purely data-driven approaches use standard neural network architectures as a so-called black box to learn the mapping between the input (ie, the acquired undersampled k-space data) and the desired output (ie, the reconstructed MRI sequence), thereby heavily relying on a huge amount of data to train the black box without use of any previous knowledge.[25] In contrast, the model-driven dCNN approaches, which were also adopted in our study, explicitly include the physical relationship between the input (ie, the acquired undersampled k-space data) and the desired output (ie, the reconstructed MRI sequences) thereby providing two major advantages over data-driven approaches: (1) they are less prone to introduction of false or unexplainable

structures on images, known as hallucinations, when reconstructing MRI images from k-space data due to explicit constraint between the reconstructed image and the observed data even at test time, and (2) the inclusion of this physical constraint reduces the number of training parameter required for reconstruction which also reduces the number of training samples required for training.[24,26] Major MRI scanner manufacturers have developed their own deep learning-based MRI acceleration algorithms,[27,28] but they differ from the architecture discussed here. These manufacturer-specific algorithms mainly involve image denoising or super-resolution networks, or both, reducing scan time by capturing only low frequency data followed by denoising, which leads to a low resolution scan followed by image super resolution. Additionally, vendor-neutral post-processing algorithms for image super-resolution also follow this principle,[29] but they operate on the final output rather than raw data. These super-resolution based methods require more training data to learn accurate reconstruction, and might be prone to generate results that are unrealistic because there is no explicit constraint on fidelity between super-resolved image and the acquired data.[30] Unlike these approaches, the architecture in our study does exploit the low-dimensional manifold of MRI images, potentially allowing more accurate and realistic reconstructions and enabling higher acceleration rates. An in-depth discussion of different MRI reconstruction algorithms and comparison with our dCNN is in the appendix (p 8).

Our study has some limitations. First, we acknowledge the retrospective nature of our study, which necessitated conducting our experiments on simulated, retrospectively generated k-space data, except for the multi-coil fastMRI dataset. Specifically, the k-space data, which holds the MRI raw data before reconstruction into visually perceivable images (ie, the MRI sequences), is not routinely stored and therefore per se not available from retrospective data. However, by applying a fast Fourier transform algorithm, MRI can still be retrospectively converted to the k-space data. Although this approach allowed us to leverage available large-scale datasets for developing MRI reconstruction techniques, it came with some limitations. The MRI data in the present study were derived from more than 200 unique institutions and MRI hardware and acquisition parameters might be different between institutions. Specifically, some of the MRI data might have been acquired using multi-coil (parallel) imaging, whereby several receiver coils are used to capture the MRI signal, which means that each of the receiver coils only needs to partially sample the k-space. However, the retrospective experiment could only accurately imitate single-coil image acquisition because all the scan's parameters (specifically coil sensitivity maps, which encompass each coil's unique contribution to specific parts of the image to create the final image) were not readily available. This unavailability affects the effective acceleration rate, because the multi-coil (parallel) image acquisition would already have an acceleration factor typically in the range of approximately 2–3.[6–8] Consequently, the net acceleration of the developed dCNN with 10-times undersampling would be in the range of 3·3 to 5 for multi-coil (parallel) image acquisition. Moreover, modern MRI machines use denoising algorithms to improve the quality of final output MRI sequence, hence the k-space retrospectively estimated from final MRI sequences will also be affected with this operation. Despite these theoretical limitations when using retrospectively generated k-space data for experiments, we show that the dCNN shows excellent generalisability when applied (without retraining) to prospectively available raw k-space data from the fastMRI brain cohort. Specifically, the dCNN had excellent performance when reconstructing MRI both for single-coil and multi-coil MRI acquisition, also in comparison with the best performing models of the fastMRI challenge.[10] The generalisability is facilitated by the design of the dCNN model, specifically the data consistency block (conjugate gradient block), which explicitly enforces the constraint that the k-space of a reconstructed image should match the undersampled k-space data at sampling locations. Second, we acknowledge that future studies should focus not only on quantitative metrics, but also on the assessment of qualitative measurements as perceived by human readers (radiologists), which might be important to provide a more comprehensive evaluation. Third, we acknowledge that for prospective clinical adoption the dCNN model would need to be embedded into the software platform used for operating the MRI scanner to allow seamless reconstruction of MRI from the acquired undersampled k-space data. To facilitate this process, we have made our trained dCNN model available as open source, thereby encouraging other researchers and developers to build on our work and accelerate the translation from research into clinical application.

For more on **our trained dCNN model** see www.github.com/neuroAI-HD/dCNN-MRI-Reconstruction

In conclusion, deep-learning-based reconstruction of undersampled MRI allows a substantial reduction of scan times surpassing the capabilities of conventional MRI acceleration methods. With acceleration by a factor of 10, this method demonstrates excellent image quality while preserving the accuracy of derived imaging biomarkers for the assessment of oncological treatment response. Our model is available online and holds considerable promise for accelerating MRI, which will be particularly advantageous in resource-constrained settings, and ultimately might increase accessibility to MRI.

Contributors

PV and ARas designed the study. ARas performed development, training, and application of the dCNN. PV, ARas, GB, CJP, MAM, MF-D, IP, and MS performed preprocessing of MRI data in the HD, CENTRIC, CORE and EORTC-26101 cohorts. PV, ARas, MF-D, EK, and KD-H performed postprocessing of the MRI data in the fastMRI brain cohort. MJvdB, AI, MP, AAB, BN, RS, JD, TG, J-CT, MW, WW, and MB critically contributed to the primary analysis of the relevant data from the

CENTRIC, CORE and EORTC-26101 trials, which were used within the present study. PV, ARas, and TG performed statistical analyses. PV and ARas interpreted the findings with essential input from all coauthors. PV and ARas prepared the first draft of the manuscript. All authors critically revised the manuscript for important intellectual content. All authors approved the final version of the manuscript. PV and ARas accessed and verified all the data. All authors had access to all the data in the study, and all authors had final responsibility for the decision to submit for publication.

Declaration of interests

AI reports grants from Carthera, Transgene, Nutrithéragène, and Sanofi; consulting fees from Novocure, Leo Pharma, Novartis and Boehringer Ingelheim; support for attending meetings from Carther and Enterome; and participation in Data Safety Monitoring for NCT02331498, outside the submitted work. DB reports consulting fees from Novocure and AdBoard; and honoraria for lectures from Novocure, outside of the submitted work. EK reports planned patents with the University of Bonn (Deep multi-modal learning for reduction and enhancement of GBCA contrast agent); and being a cofounder of the relios.vision, outside the submitted work. FTK reports grants from the German Research Foundation (507778602) and consulting fees from Need Inc outside the submitted work. J-CT reports grants from Novocure and Munich Surgical Imaging; consulting fees from Novartis; honoraria for lectures from Seagen; and leadership or fiduciary role in the World Federation of Neurosurgical Societies Neurooncology Committee and RANO resect committee, outside of the submitted work. JD reports grants from ViewRay, The Clinical Research Institute, Accuray, RaySearch Laboratories, Vision RT, Merck Serono, Astellas Pharma, AstraZeneca, Siemens Healthcare, Solution Akademie, Egomed, Quintiles, Pharmaceutical Research Association, Boehringer Ingelheim, PTW-Freiburg Dr Pychlau, and Nanobiotix, outside of the submitted work. KD-H reports grants from Federal Agency for Disruptive Innovations, Women TechEU, the University Bonn (Smart Contrast), Federal Ministry of Education and Research (BMBF) Grant (CureDem – Demenz besiegen), Subproject on Brain Clearance Imaging 2021, EU Joint Programme – Neurodegenerative Disease Research Grant (Human Brain Clearance Imaging), BMBF Grant (Address, Subproject 4: personalized oncologic surveillance imaging platform); honoraria for lectures from Guerbet, Bayer, and GE; and is cofounder and Chief Executive Officer of relios.vision, outside the submitted work. MB reports grants from the EU, German Research Foundation (DFG), and Novartis; consulting fees from Seagen, NeuroScios, and Boehringer Ingelheim; honoraria for lectures from Novartis, Seagen, and Boehringer Ingelheim; and has a leadership or fiduciary role as Editor-in-Chief for *Clinical Neuroradiology* (Springer), outside of the submitted work. MJvdB reports consulting fees from Genenta, Roche, Servier, Fore Biopharm, AstraZeneca, Incyte, Boehringer Ingelheim, and Chimerix; and honoraria for lectures from Servier, outside the submitted work. MP reports grants from Roche, Pfizer, and Bayer; royalties from Bayer; consulting fees from Pasithea; patents on a method of modulating cellular activity and agents useful for the same (US 7531575 B2), method of modulating T cell functioning (US 20080009519 A1), Trp/His exchange and kynurenine induced Trp transport (US 7935494 B2), means and methods for treating and/or preventing natural AHR ligand-dependent cancer (PCT/EP2012/067504, WO 2013/034685), 3-oxo-2,6-diphenyl-2,3-dihydropyridazine-4-carboxamides (EP3464248A1), and peptides for use in treating or diagnosing IDH1R132H positive cancers (EP2800580B1); participation in data safety monitoring board or advisory board for INFORM2_NivEnt, IMA950-106, Pasithea, Vaximm, Frankfurt Cancer Institute, Affiris, and BioRN; leadership or fiduciary role in the German Neuro-Oncology Working Group (NOA) and the European Association of Neuro-Oncology; stock or stock options in Twist, Agilent, 10xGenomics, Evotech, Qiagen; and has received equipment from Pfizer, Roche, and Bayer, outside the submitted work. PV reports grants from DFG, Aventis Foundation, Else Kröner Fresenius Foundation, and EUROSTARS; consulting fees and stock options from Need Inc; and participation in advisory board for Cercare Medical, outside the submitted work. RS reports consulting fees from Neosoma, outside the submitted work. WW reports consulting fees from Bayer, Roche, Servier, AstraZeneca, and Enterome; and receipt of drugs from Apogenix, Pfizer, and Roche for the N2M2/NOA-20 trial. All other authors declare no competing interests.

Data sharing

The multi-institutional data from the CENTRIC and CORE trials used for training and validation of the dCNN and the multi-institutional data from the EORTC-26101 used for independent testing of the dCNN are not publicly available and restrictions apply to their use via the EORTC external research collaboration. The fastMRI data can be obtained at https://fastmri.med.nyu.edu after completion of the NYU Langone Health fastMRI Dataset Sharing Agreement. The trained dCNN model is available at www.github.com/neuroAI-HD/dCNN-MRI-Reconstruction.

Acknowledgments

We acknowledge funding from the DFG as part of the Priority Programme 2177 Radiomics: Next Generation of Biomedical Imaging (project identifier: 428223917) and Collaborative Research Center 1389 (UNITE Glioblastoma – project identifier: 404521405). PV is funded through an Else Kröner Clinician Scientist Endowed Professorship by the Else Kröner Fresenius Foundation (reference number: 2022_EKCS.17). Parts of the MRI data used for this study were acquired through the CORE study (a Merck KGaA study), the CENTRIC study, an EORTC study supported by Merck KGaA, and the EORTC-26101 study (supported by Hoffmann-La Roche).

References

1 Hricak H, Abdel-Wahab M, Atun R, et al. Medical imaging and nuclear medicine: a *Lancet Oncology* Commission. *Lancet Oncol* 2021; **22:** e136–72.
2 O'Connor JP, Aboagye EO, Adams JE, et al. Imaging biomarker roadmap for cancer studies. *Nat Rev Clin Oncol* 2017; **14:** 169–86.
3 Hugosson J, Månsson M, Wallström J, et al. Prostate cancer screening with PSA and MRI followed by targeted biopsy only. *N Engl J Med* 2022; **387:** 2126–37.
4 Liu Y, Leong ATL, Zhao Y, et al. A low-cost and shielding-free ultra-low-field brain MRI scanner. *Nat Commun* 2021; **12:** 7238.
5 Murali S, Ding H, Adedeji F, et al. Bringing MRI to low- and middle-income countries: directions, challenges and potential solutions. *NMR Biomed* 2023; published online July 4. https://doi.org/10.1002/nbm.4992.
6 Baert A. Parallel imaging in clinical MR applications. Berlin: Springer Science & Business Media, 2007.
7 Serai SD, Hu HH, Ahmad R, et al. Newly developed methods for reducing motion artifacts in pediatric abdominal MRI: tips and pearls. *AJR Am J Roentgenol* 2020; **214:** 1042–53.
8 Nael K, Ruehm SG, Michaely HJ, et al. High spatial-resolution CE-MRA of the carotid circulation with parallel imaging: comparison of image quality between 2 different acceleration factors at 3.0 Tesla. *Invest Radiol* 2006; **41:** 391–99.
9 Lavrenko A, Römer F, Del Galdo G, Thomä R. On the SNR variability in noisy compressed sensing. *IEEE Signal Process Lett* 2017; **24:** 1148–52.
10 Muckley MJ, Riemenschneider B, Radmanesh A, et al. Results of the 2020 fastMRI challenge for machine learning MR image reconstruction. *IEEE Trans Med Imaging* 2021; **40:** 2306–17.
11 Knoll F, Murrell T, Sriram A, et al. Advancing machine learning for MR image reconstruction with an open competition: overview of the 2019 fastMRI challenge. *Magn Reson Med* 2020; **84:** 3054–70.
12 Nabors LB, Fink KL, Mikkelsen T, et al. Two cilengitide regimens in combination with standard treatment for patients with newly diagnosed glioblastoma and unmethylated *MGMT* gene promoter: results of the open-label, controlled, randomized phase II CORE study. *Neuro-oncol* 2015; **17:** 708–17.
13 Stupp R, Hegi ME, Gorlia T, et al. Cilengitide combined with standard treatment for patients with newly diagnosed glioblastoma with methylated *MGMT* promoter (CENTRIC EORTC 26071-22072 study): a multicentre, randomised, open-label, phase 3 trial. *Lancet Oncol* 2014; **15:** 1100–08.
14 Wick W, Gorlia T, Bendszus M, et al. Lomustine and bevacizumab in progressive glioblastoma. *N Engl J Med* 2017; **377:** 1954–63.
15 Wick W, Stupp R, Gorlia T, et al. Phase II part of EORTC study 26101: the sequence of bevacizumab and lomustine in patients with first recurrence of a glioblastoma. *Proc Am Soc Clin Oncol* 2016; **34** (suppl)**:** 2019 (abstr).
16 Zbontar J, Knoll F, Sriram A, et al. fastMRI: an open dataset and benchmarks for accelerated MRI. *arXiv* 2018; published online Nov 21. https://doi.org/10.48550/arXiv.1811.08839 (preprint).

17 Mongan J, Moy L, Kahn CE Jr. Checklist for artificial intelligence in medical imaging (CLAIM): a guide for authors and reviewers. *Radiol Artif Intell* 2020; **2:** e200029.

18 von Elm E, Altman DG, Egger M, Pocock SJ, Gøtzsche PC, Vandenbroucke JP. The strengthening the reporting of observational studies in epidemiology (STROBE) statement: guidelines for reporting observational studies. *Lancet* 2007; **370:** 1453–57.

19 Aggarwal HK, Mani MP, Jacob M. MoDL: Model-based deep learning architecture for inverse problems. *IEEE Trans Med Imaging* 2019; **38:** 394–405.

20 Langkammer C, Schweser F, Shmueli K, et al. Quantitative susceptibility mapping: report from the 2016 reconstruction challenge. *Magn Reson Med* 2018; **79:** 1661–73.

21 Kickingereder P, Isensee F, Tursunova I, et al. Automated quantitative tumour response assessment of MRI in neuro-oncology with artificial neural networks: a multicentre, retrospective study. *Lancet Oncol* 2019; **20:** 728–40.

22 Ellingson BM, Wen PY, Cloughesy TF. Modified criteria for radiographic response assessment in glioblastoma clinical trials. *Neurotherapeutics* 2017; **14:** 307–20.

23 Landis JR, Koch GG. The measurement of observer agreement for categorical data. *Biometrics* 1977; **33:** 159–74.

24 Zeng G, Guo Y, Zhan J, et al. A review on deep learning MRI reconstruction without fully sampled k-space. *BMC Med Imaging* 2021; **21:** 195.

25 Liang D, Cheng J, Ke Z, Ying L. Deep MRI reconstruction: unrolled optimization algorithms meet neural networks. *arXiv* 2019; published online July 26. https://doi.org/10.48550/arXiv.1907.11711 (preprint).

26 Hendriks J, Jidling C, Wills A, Schön T. Linearly constrained neural networks. *arXiv* 2020; published online Feb 5. https://doi.org/10.48550/arXiv.2002.01600 (preprint).

27 Behl N. Deep resolve—mobilizing the power of networks. 2021. https://marketing.webassets.siemens-healthineers.com/15fe3041cb84f0c0/c102fcc011dd/Behl_Deep-Resolve_MAGNETOM_Flash_78_ISMRM_2021.pdf (accessed Jan 30, 2024).

28 Lebel RM. Performance characterization of a novel deep learning-based MR image reconstruction pipeline. *arXiv* 2020; published online Aug 14. https://doi.org/10.48550/arXiv.2008.06559 (preprint).

29 Rudie JD, Gleason T, Barkovich MJ, et al. Clinical assessment of deep learning-based super-resolution for 3D volumetric brain MRI. *Radiol Artif Intell* 2022; **4:** e210059.

30 Shlezinger N, Whang J, Eldar YC, Dimakis AG. Model-based deep learning. *Proc IEEE* 2023; **111:** 465–99.